MATERIALS PHYSICS AND MECHANICS RESEARCH ARTICLE

Submitted: October 13, 2024 **Revised: November 5, 2024** **Accepted: December 16, 2024**

Modeling of working cycles of thermomechanical actuators based on shape memory alloys at repeated actuation

F.S. Belyaev [1]✉, A.E. Volkov [2], D.F. Gorbachenko [2], M.E. Evard [2]

[1] Institute for Problems of Mechanical Engineering RAS, St. Petersburg, Russia

[2] St. Petersburg State University, St. Petersburg, Russia

✉ belyaev_fs@mail.ru

ABSTRACT

The microstructural model of the mechanical behavior of shape memory alloys was applied to describe the operation of a thermomechanical torsion actuator with a TiNi alloy working body and an elastic counterbody. The calculated dependences of a recovery strain, maximum stress in a cycle, and irreversible deformation on the cycle number were plotted for the working body of the actuator. It is shown that from cycle to cycle there is an accumulation of irreversible deformation, the rate of which gradually decreases. As a consequence, both the value of a recovery strainand the value of the stresses developed by the actuator decrease, which together leads to a decrease in the work output. The influence of the stiffness of the elastic counterbody on the specific work produced in the cycle was investigated. It is shown that the produced work depends non-monotonically on the stiffness of the counterbody and there is an optimal stiffness at which this work is maximized.

KEYWORDS

shape memory alloys • actuator • microstructural modeling • plastic deformation • TiNi

Acknowledgements. *The research was carried out within the state assignment of Ministry of Science and Higher Education of the Russian Federation (theme No. 124041500009-8).*

Citation: Belyaev FS, Volkov AE, Gorbachenko DF, Evard ME. Modeling of working cycles of thermomechanical actuators based on shape memory alloys at repeated actuation. *Materials Physics and Mechanics*. 2024;52(6): 81–90.
http://dx.doi.org/10.18149/MPM.5262024_7

Introduction

Currently, actuators with working bodies made of shape memory alloys (SMA) are being actively developed and manufactured [1–16]. One of the main sources of interest in such actuators is the strict requirements for the weight of the product in modern aircraft, spacecraft, and various robotic systems. SMA-based actuators allow achieving a weight gain of up to 80 % compared to similar electric and hydraulic actuators [11]. In addition, SMA-based actuators are highly reliable, have high rates of developed forces, are quiet in operation, have a simple design, and have a small number of moving parts. At the same time, SMAs can be equally well used in large actuators that develop significant forces, as well as in microactuators.

The operation of a thermomechanical actuator with SMA working bodies is based on the implementation of the shape memory effect – the restoration of deformation during heating. Accordingly, when the working body cools, the actuator must return to its initial state. The restoration of the initial deformation occurs due to the effect of transformation plasticity, which is realized when an external load is applied during

cooling. Thus, the working cycle consists of two stages: the "cocking" stage, when the working body accumulates deformation and the actuation stage, when the deformation of the working body is restored. Actuator designs can be different, but we can distinguish between double-sided actuators capable of developing forces in two opposite directions, and single-sided actuators, with a working stroke in one direction. Double-sided actuators usually use two working bodies made of SMA, which alternately perform a working stroke, simultaneously cocking each other [14–16]. But more often, single-sided actuators are used, the design of which usually includes a SMA working body, which performs useful work when heated, and an elastic counterbody, which restores the initial deformation of the working body when cooled due to the stored elastic energy.

Despite the many advantages of SMA-based actuators, they have some drawbacks. The main drawback is the instability of the functional properties of SMA. Multiple implementation of the actuator's working cycle leads to the accumulation of irreversible deformation, a change in the characteristic temperatures of martensitic transformations, a decrease in the magnitude of the recoverable deformation and the developed forces [17]. This phenomenon manifests in all SMAs, the scale of changes depends on many factors, such as the alloy composition, the type of transformation, preliminary thermomechanical treatment, the magnitude of the acting load during the transformation, etc. [18–22]. Instability of properties can lead to a decrease in the useful work produced in the actuator's working cycle or to its incomplete operation.

Successful design of SMA-based actuators requires reliable tools of calculating the features of their mechanical behavior, including the instability of SMA properties. In known studies [15,16,23,24], simplified approaches and simple models are used to describe the behavior of the working element, which only allow one to approximately determine the actuator characteristics. On the other hand, there are microstructural models that can describe all the functional properties of SMA [25–28]. This class of models has a high predictive power and is capable of describing changes in SMA properties under repeated thermomechanical effects. But these models are not simple and transparent enough, and using them to solve specific problems requires additional efforts. In this regard, the purpose of this work was to study the possibility of using a microstructural model to describe the operation of a thermomechanical actuator based on SMA.

Microstructural model

To describe the mechanical behavior of SMA, the microstructural model developed earlier by the authors [28–32] was used in the present work. The representative volume considered within its framework corresponds to the material point of the material. The microstructural model implies the existence of several structural levels, which, in order to better describe the alloy behavior, should reflect the actual microstructure of the material. In the proposed model, it is considered that the representative volume consists of grains with different orientations of the crystallographic axes, which, in turn, consist of volumes occupied by austenite and/or orientational variants of martensite.

According to the Reuss hypothesis, the deformation of the representative volume is calculated by orientational averaging of the deformations of the grains that compose it:

$$\varepsilon = \sum_{\omega} f(\omega)\varepsilon^{gr}(\omega), \quad (1)$$

where ω is the orientation of crystallographic axes, $f(\omega)$ is the volume fraction of grains with orientation ω, and $\varepsilon^{gr}(\omega)$ is the deformation of these grains. The grain deformation can be represented as the sum of contributions of individual deformation mechanisms:

$$\varepsilon^{gr} = \varepsilon^{E} + \varepsilon^{T} + \varepsilon^{Ph} + \varepsilon^{MP}, \quad (2)$$

where ε^{E} is elastic deformation determined by Hooke's law, ε^{T} is temperature deformation due to thermal expansion, ε^{Ph} is phase deformation, ε^{MP} is microplastic deformation.

To describe the phase deformation, the model introduces internal variables Φ_n such that Φ_n/N is the volume fraction of the n-th martensite variant, where N is the number of possible martensite variants. The grain phase deformation ε^{Ph} is calculated by averaging over all martensite variants:

$$\varepsilon^{Ph} = \frac{1}{N}\sum_{n=1}^{N} \Phi_n D^n, \quad (3)$$

where D^n is the Bain strain tensor for the n-th variant of martensite.

The martensitic transformation condition is as follows:

$$F_n = \pm F^{fr}, \quad (4)$$

where F_n is the generalized thermodynamic force causing the growth of the n-th variant of martensite, F^{fr} is the dissipative force preventing the movement of interphase boundaries and responsible for the presence of temperature-phase hysteresis, the "+" sign corresponds to the direct transformation, and "-"to the reverse one.

The growing martensitic crystal, due to the incompatibility of its deformation with the austenitic matrix, creates internal stresses causing microplastic deformation. When calculating this microplastic deformation, the main assumption is that the microplastic deformation generated by the growth of a certain martensite variant is proportional to the deviator of the Bain deformation of this variant:

$$\varepsilon^{MP} = \frac{1}{N}\sum_{n=1}^{N} \kappa\varepsilon_n^{mp} dev(D^n), \quad (5)$$

where ε_n^{mp} is the scalar measure of microplastic deformation associated with the growth of the n-th martensite variant, κ is the scale factor for microplastic deformation.

The conditions for the onset of microplastic yield are similar to those for plastic yield in the one-dimensional case, taking into account kinematic and isotropic hardening, where the role of stress is played by the generalized thermodynamic force F_n^p, and the thermodynamic forces F^y and F_n^ρ correspond to kinematic and isotropic hardening:

$$\left|F_n^p - F_n^\rho\right| = F^y, \quad \left(F_n^p - F_n^\rho\right)dF_n^p > 0, \quad (6)$$

the generalized thermodynamic force causing microplastic deformation is calculated as follows:

$$F_n^p = \mu\sum_{m=1}^{N} A_{mn}(\Phi_m - b_m), \quad (7)$$

where b_m is the density of oriented defects, A is the matrix defining the interaction of martensite variants described in detail in [33,34], and the coefficient μ is calculated as follows:

$$\mu = -\frac{q_0(M_s - M_f)}{T_0(1-2\alpha)}, \quad (8)$$

$$T_0 = \frac{M_s + A_f}{2}, \quad (9)$$

where q_0 is the latent heat of transformation, M_s and M_f are the temperatures of the beginning and end of direct martensitic transformation, A_f is the temperature of the end of reverse transformation, T_0 is the thermodynamic equilibrium temperature of the phases (austenite and martensite), α is the interaction coefficient of martensite variants.

Deformation defects resulting from microplastic yielding can be divided into two groups: oriented defects, which create long-range stress fields, and scattered defects. To calculate the densities of oriented defects b_n and scattered defects f, the following evolution equations are proposed:

$$\dot{b_n} = \dot{\varepsilon}_n^{mp} - \frac{1}{\beta^*}|b_n|\dot{\varepsilon}_n^{mp} H\left(b_n \dot{\varepsilon}_n^{mp}\right), \quad (10)$$

$$\dot{f} = \sum_{m=1}^{N} |\dot{\varepsilon}_m^{mp}| + r_1(f - f_0)\Phi^{gr} H(-\Phi^{gr}), \quad (11)$$

where H is the Heaviside function, β^* is the maximum density of oriented defects in grain, r_1 is the recovery coefficient of scattered defects, f_0 is the equilibrium value of scattered defects.

In order to obtain a closed system of equations that allows the calculation of all internal variables, it is necessary to introduce hardening laws. In the model, it is considered that scattered defects impede the movement of dislocations and thereby create isotropic hardening, and pile-ups of oriented defects, generating internal stress fields, create kinematic hardening. Linear dependences are proposed to relate hardenings to defect densities:

$$F_n^{\rho} = a_{\rho} b_n\,, \quad (12)$$

$$F^{y} = a_y f, \quad (13)$$

where a_ρ and a_y are the kinematic and isotropic hardening coefficients, respectively.

Simulation results

The object of the study was a torsion actuator with a TiNi alloy working body and an elastic counterbody. In order for the actuator's working body to recover deformation and generate stress upon heating, it needs to be given an initial strain. In the simulated experiments, the sample was pre-strained in the martensitic state to 7 % and connected to an elastic counterbody of a given stiffness after unloading. Then, heating up to 450 K caused the working stroke of the actuator (deformation recovery and stress increase), and cooling to 300 K caused cocking (increase in strain and decrease in stress). In the strain-stress coordinates, a linear trajectory corresponds to the working stroke and cocking. The slope of this line is determined by the stiffness of the counterbody. The scheme of preparation of the actuator working body and its functioning is shown in Fig. 1.

To verify the ability of the presented model to describe the behavior of SMA under thermomechanical actuator conditions, numerical experiments corresponding to real experiments from [17] for a single-sided actuator with working element made of TiNi alloy and elastic counterbody were carried out. In the model, a particular alloy is defined

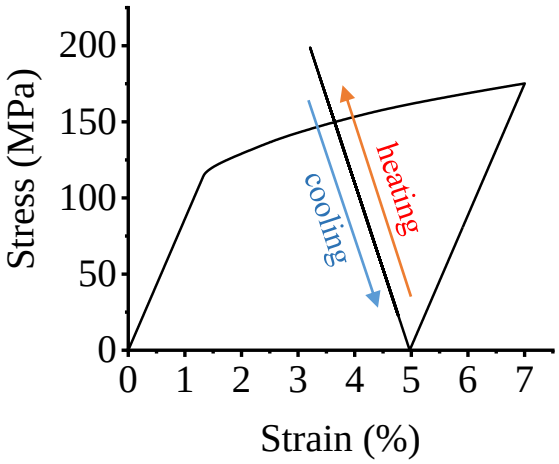

Fig. 1. The scheme of initial preparation of the actuator working body and its functioning under thermocycling

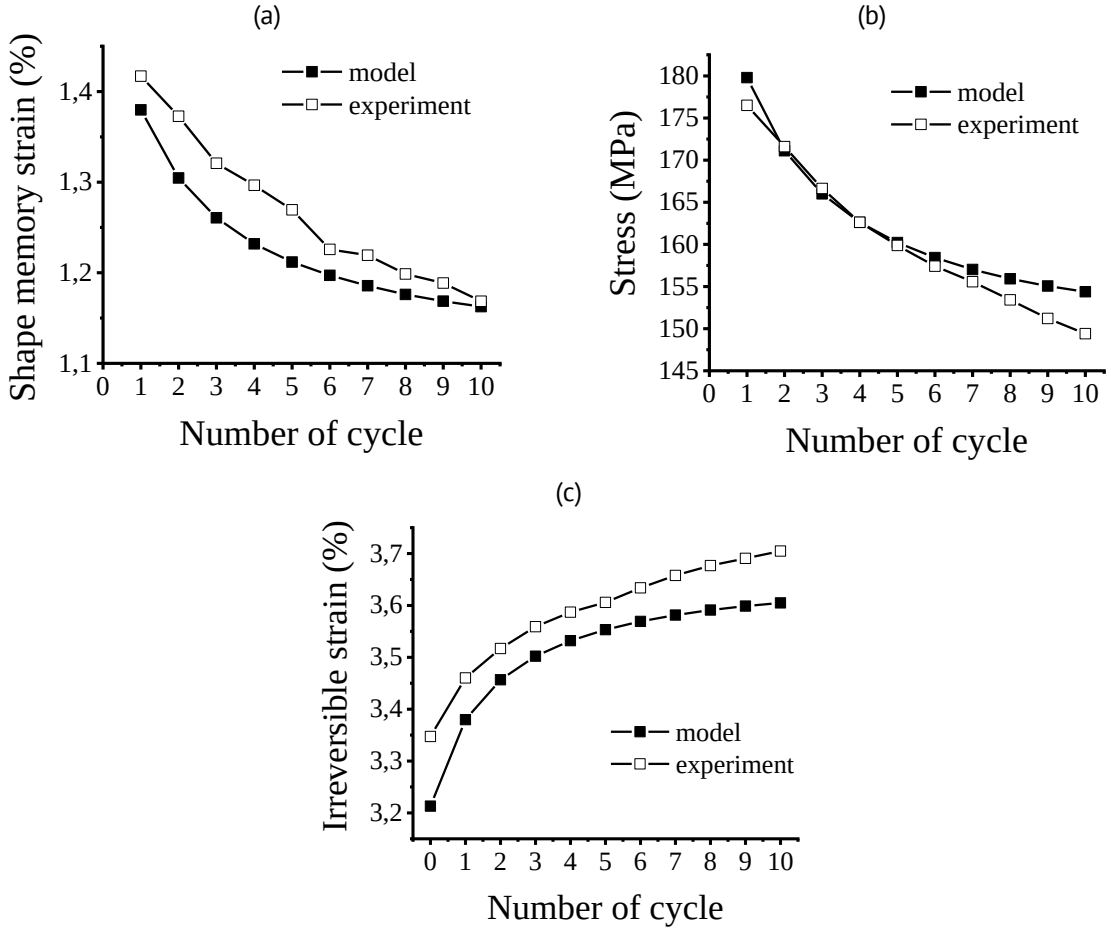

Fig. 2. The evolution of a recovery strain (a) stresses developed by the actuator (b) and accumulated residual strain (c) at thermocycling for the actuator with a counterbody stiffness of 11.3 GPa

by a corresponding set of material constants. For the calculations, characteristic temperatures and latent heat of martensite transformations were taken directly from [17], a temperature of the thermodynamic equilibrium was calculated by Eq. (9), a number of martensite variants corresponds to B2↔B19' martensitic transformation realized in TiNi

alloys, other constants were fitted to best describe the change in the working cycle parameters of the actuator with a counterbody stiffness of 11.3 GPa at the first ten actuations. The considered cycle parameters included: a recovery strain i.e. strain recovered by heating (Fig. 2(a)), maximum stresses developed by the actuator (Fig. 2(b)), accumulated residual strain (Fig. 2(c)). In Fig. 2, it can be seen that the selected constants allowed the model to describe well the evolution of the considered parameters of the actuator working cycle for the first ten operations. The list of material constants used for modeling is presented in Table 1.

Table 1. Material constants for TiNi alloy

Material constant	Symbol	Value
Number of martensite variants	N	12
Latent heat (enthalpy) of the direct martensitic transformation, MJ/m^3	q_0	-160
Characteristic temperatures of martensite transformation, K	M_f M_s A_s A_f	310 332 340 363
Temperature of the thermodynamic equilibrium, K	T_0	347.5
interaction coefficient of martensite variants	α	0.2
Microplastic strain scaling factor	κ	1
Coefficient of isotropic hardening, MPa	a_y	1
Coefficients of kinematic hardening, MPa	a_ρ	10
Maximum value of the oriented defects density	β^*	0.6
Initial value of scattered defects	f_0	0
Scattered defects recovery coefficient	r_1	0

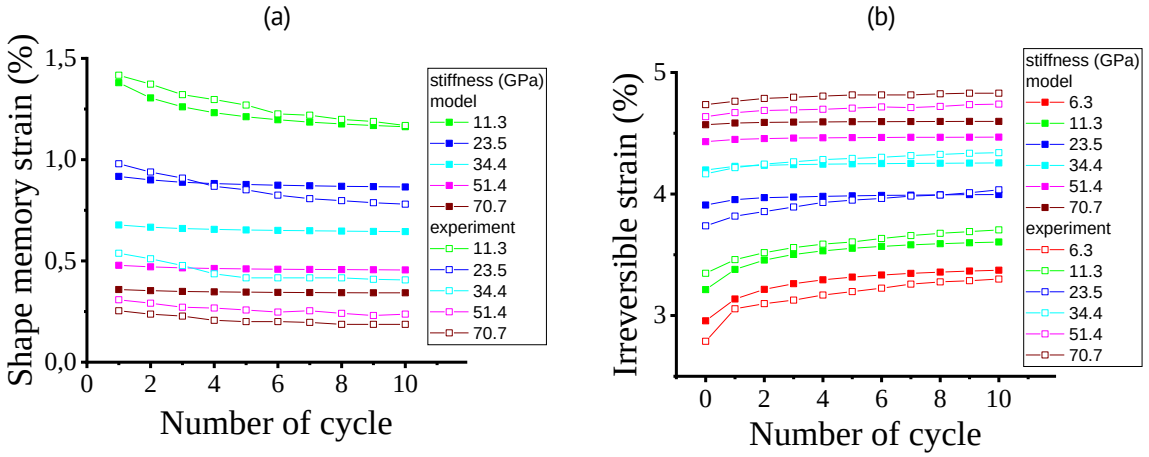

Fig. 3. The evolution of a recovery strain (a) and accumulated residual strain at thermocycling

To verify the predictive power of the model, numerical experiments were performed for other counterbody stiffnesses. Figure 3 shows a comparison of the calculated and experimental strain dependences of the shape memory effect and the accumulated residual strain for the first ten cycles. Figure 3(a) demonstrates that the model predicts very well the evolution of a recovery strain up to stiffness 23.5 GPa. For larger values of the counterbody stiffness there are some numerical discrepancies, but nevertheless there

is a good qualitative agreement. Similar results were obtained for irreversible deformation (see Fig. 3(b)), good agreement is observed up to a stiffness of 34.4 GPa, and for larger values there is a quality compliance. Thus, the model with a single set of material constants allows obtaining good results for stiffnesses close to 11.3 GPa (for which the constants were selected), and for the rest it gives a qualitative agreement.

According to experimental data [17], a significant portion of the residual strain appears during the preparation of the working element (preliminary deformation and first heating – cycle 0 in Fig. 3(b)), and then it gradually increases from cycle to cycle. It is also noted that with high counterbody stiffness, more irreversible deformation accumulates during the preparation process, but then it grows insignificantly. Since the accumulation of irreversible deformation leads to a decrease in a recovery strain, then with high stiffness values it also exhibits greater stability. These features of the operation of actuators with different counterbody stiffness can be described using the proposed model.

To determine the efficiency of the actuator, the amount of specific work produced during heating must be estimated. It can be calculated by the equation:

$$A = \frac{\tau^r \gamma^{sm}}{2}, \tag{14}$$

where γ^{sm} is the a recovery strain and τ^r is the stresses developed by the actuator.

The calculation of the influence of the counterbody stiffness on a recovery strain and the stresses developed by the actuator are shown in Figs. 4(a) and 4(b), respectively. It can be seen that a recovery strain decreases with increasing counterbody stiffness, while the stresses developed by the actuator increase. Since the specific work of the actuator is proportional to both of these quantities, the antidirectionality of the dependencies makes the choice of the optimal counterbody stiffness non-obvious. It can also be noted that thermal cycling leads to a decrease in both the recovered strain and the developed stresses regardless of the stiffness of the counterbody. Therefore, it can be concluded that the specific work of the actuator will gradually decrease during the operation of the actuator.

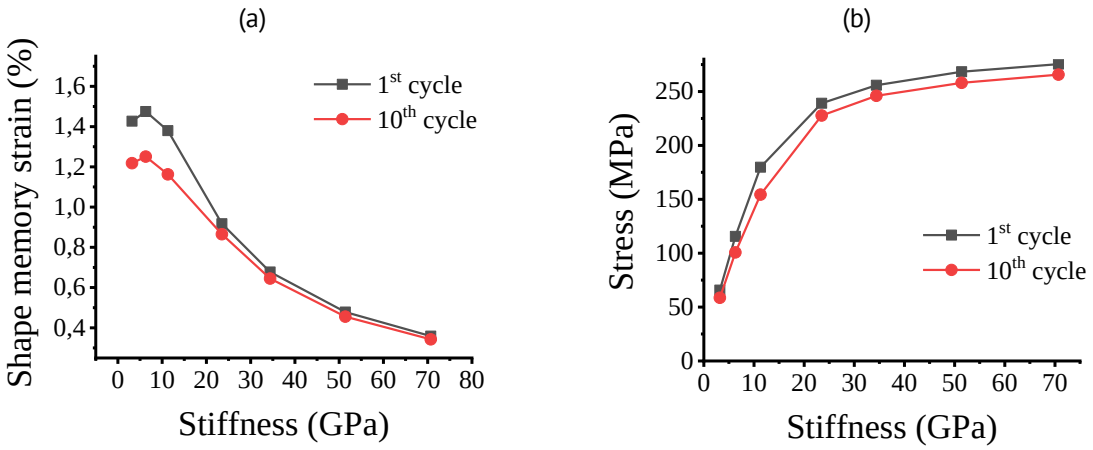

Fig. 4. The dependences of a recovery strain (a) and stresses developed by the actuator (b) on stiffness of counterbody for first and tenth cycle

A series of numerical experiments were carried out to find out the optimum stiffness to obtain the highest specific work. The calculated data presented in Fig. 5(a) qualitatively correspond to similar experimental data [17], which are presented in Fig. 5(b). As can be seen in Fig. 5(a) the specific work of the actuator changes non-monotonically as the stiffness of the counterbody increases. There is an optimal stiffness in the range of 10-15 GPa. As mentioned above changes occurring in the alloy during thermal cycling negatively affect the work produced by the actuator, but they practically do not change the optimum stiffness (see Fig. 5(a)).

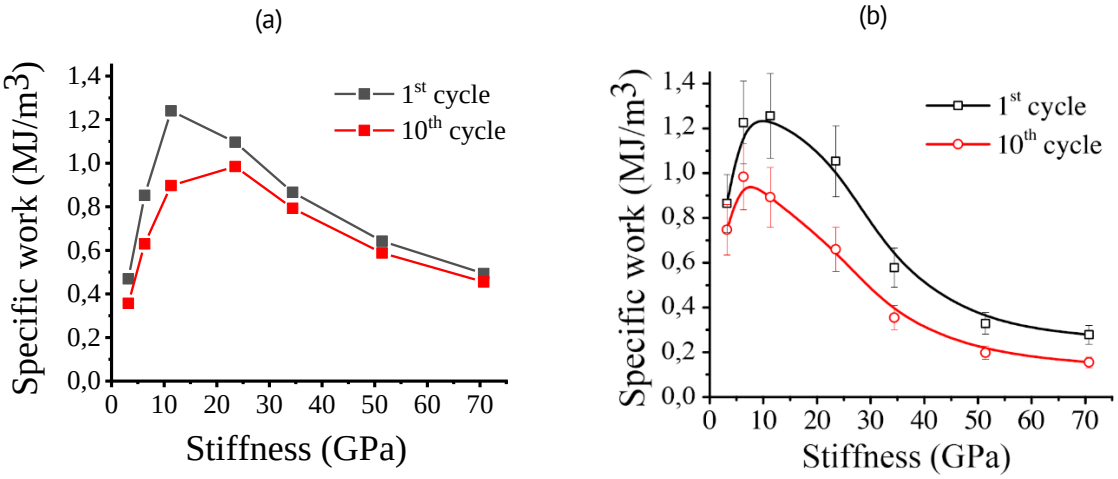

Fig. 5. The dependence of specific work on stiffness of counterbody for first and tenth cycle, simulation (a) and experiment [17] (b)

The existence of a maximum of the work produced is an interesting result and is explained in [17] as follows. The useful work depends on the magnitudes of the recovered strain and the developed stresses, but when the working element is heated during the working stroke, these magnitudes are related. In the absence of counteraction, when the developed stresses equal to zero, the largest recoverable strain is achieved. The highest reactive stresses are achieved under condition of absolutely constraint displacements, i.e. when the recoverable strain is zero. It follows that, in both extreme cases, the work produced by the SMA element is equal to zero. However, in the intermediate cases, there are both recoverable strain and reactive stresses and accordingly the actuator produces positive work. Hence, there is possible to find the optimal combination of developed stresses and recoverable deformations (determined by the stiffness of the counterbody) which provide the maximum work output.

Conclusions

The presented microstructural model is able to quantitatively describe and predict the deformation behavior of SMA under the operating conditions of the thermomechanical actuator. It makes it possible to describe the evolution of the actuator working cycle parameters at multiple actuations and the peculiarities of the working element behavior at different counterbody stiffnesses. Results of numerical experiments are in good agreement with experimental data.

The model allows to calculate the performance of the actuator in the first cycle and after multiple actuations. It also makes it possible to describe the non-monotonic variation of the specific work as a function of the counterbody stiffness and thus can be used to optimize the actuator working cycle.

References

1. Mohd Jani J, Leary M, Subic A, Gibson MA. A review of shape memory alloy research, applications and opportunities. *Materials & Design*. 2014;56: 1078-1113.
2. Butera F, Coda A, Vergani G. Shape memory actuators for automotive applications. In: *Proc. of the Intern. Conf. "Nanotec IT newsletter"*. 2007. p.12–16.
3. Hartl DJ, Lagoudas DC. Aerospace applications of shape memory alloys. *J. of Aerospace Engineering*. 2007;221(4): 535–552.
4. Kheirikhah MM, Rabiee S, Edalat ME. A Review of Shape Memory Alloy Actuators in Robotics. In: Ruiz-del-Solar J, Chown E, Plöger PG. [eds.] *RoboCup 2010: Robot Soccer World Cup XIV. RoboCup 2010. Lecture Notes in Computer Science, Vol. 6556*. Berlin: Springer; 2011. p.206–217.
5. Yadav SK, Bobade RS. Shape Memory Alloy Actuators: A Review. *International Journal for Research in Applied Science and Engineering Technology*. 2019;7(V): 799–802.
6. Gangil N, Siddiquee AN, Maheshwari S. Towards applications, processing and advancements in shape memory alloy and its composites. *Journal of Manufacturing Processes*. 2020;59: 205–222.
7. Liu Q, Ghodrat S, Huisman G, Jansen KMB. Shape memory alloy actuators for haptic wearables: A review. *Materials & Design*. 2023;233: 112264.
8. Hamid QY, Wan Hasan WZ, Azmah Hanim MA, Nuraini AA, Hamidon MN, Ramli HR. Shape memory alloys actuated upper limb devices: A review. *Sensors and Actuators Reports*. 2023;5: 100160.
9. Lu Y, Xie Z, Wang J, Yue H, Wu M, Liu Y. A novel design of a parallel gripper actuated by a large-stroke shape memory alloy actuator. *International Journal of Mechanical Sciences*. 2019;159: 74–80.
10. Xu J, Kimura Y, Tsuji K, Abe K, Shimizu T, Hasegawa H, Mineta T. Fabrication and characterization of SMA film actuator array with bias spring for high-power MEMS tactile display. *Microelectronic Engineering*. 2020;227: 111307.
11. NASA. *NASA tests new alloy to fold wings in flight*. Available from: https://www.nasa.gov/centers/armstrong/feature/nasa-tests-new-alloy-to-fold-wings-in-flight.html
12. Ostropiko ES, Razov AI. Functional properties of TiNi conical workingelements in the holding and release device. *Cybern. Phys.* 2018;7: 216–219.
13. Ostropiko E, Razov A, Cherniavsky A. Investigation of TiNi shape memory alloy for thermosensitive wire drive. *MATEC Web Conf.* 2015;33: 03021.
14. Yang J, Zhang Y, Gu X, Li J, Fang P, Yang X, Wang J, Zhu J, Zhang W. Bi-direction and flexible multi-mode morphing wing based on antagonistic SMA wire actuators. *Chinese Journal of Aeronautics*. 2024;37(12): 373–387.
15. Pei YC, Wang XY, Yao ZY, Wang BH, Liao Z, Lu H. The driving characteristics of bidirectional SMA wire actuators - Theoretical modeling and experimental testing. *Sensors and Actuators A: Physical*. 2024;372: 115328.
16. Priadko AI, Pulnev SA, Nikolaev VI, Rogov AV, Shmakov AO, Golyandin SN, Chikiryaka AV. Investigation of single crystal Cu-Al-Ni alloy bending force elements for linear motors. *Materials Physics and Mechanics*. 2016;29(2): 158–165.
17. Sibirev A, Belyaev S, Resnina N. The influence of counter-body stiffness on working parameters of NiTi actuator. *Sensors and Actuators A: Physical*. 2021;319: 112568.
18. Belyaev S, Resnina N, Zhuravlev R. Deformation of Ti-51.5 at.%Ni alloy during thermal cycling under different thermal-mechanical conditions. *Journal of Alloys and Compounds*. 2013;577: S232–S236.
19. Furuya Y, Park YC. Thermal cyclic deformation and degradation of shape memory effect in Ti-Ni alloy. *Nondestructive Testing and Evaluation*. 1992;8–9(1–6): 541–554.
20. Hamilton RF, Sehitoglu H, Efstathiou C, Maier HJ. Mechanical response of NiFeGa alloys containing second-phase particles. *Scripta Materialia*. 2007;57: 497–499.
21. Morgan NB, Friend CM. A review of shape memory stability in NiTi alloys. *J. Phys. IV France*. 2001;11(PR8): Pr8-325-Pr8-332.
22. Sehitoglu H, Wu Y, Patriarca L. Shape memory functionality under multi-cycles in NiTiHf. *Scripta Materialia*. 2017;129: 11–15.

23. Averkin AI, Yakushev PN, Trofimova EV, Zograf GP, Timashov RB, Pulnev SA, Kustov SB, Nikolaev VI. Shape memory deformation recovery features in Cu-Al-Ni single crystals. *Materials Physics and Mechanics*. 2015;22(1): 64–68. (In Russian)
24. Jani JM, Huang S, Leary M, Subic A. Numerical modeling of shape memory alloy linear actuator. *Comput Mech*. 2015;56: 443–461.
25. Chemisky Y, Duval A, Patoor E, Ben Zineb T. Constitutive model for shape memory alloys including phase transformation, martensitic reorientation and twins accommodation. *Mechanics of Materials*. 2011;43(7): 361–376.
26. Yu C, Kang G, Song D, Kan Q. Effect of martensite reorientation and reorientation-induced plasticity on multiaxial transformation ratchetting of super-elastic NiTi shape memory alloy: New consideration in constitutive model. *International Journal of Plasticity*. 2015;67: 69–101.
27. Song D, Yu C, Zhang C, Kang G. Superelasticity degradation of NiTi shape memory alloy in wide ranges of temperature and loading level: Experimental observation and micromechanical constitutive model. *International Journal of Plasticity*, 2023;161: 103487.
28. Belyaev FS, Volkov AE, Evard ME. Microstructural modeling of fatigue fracture of shape memory alloys at thermomechanical cyclic loading. *AIP Conference Proceedings*. 2018;1959: 070003.
29. Belyaev FS, Evard ME, Volkov AE. Simulation of the plastic deformation of shape memory alloys considering shear anisotropy on the slip plane. *Materials Physics and Mechanics*. 2023;51(1): 61–67.
30. Resnina NN, Ivanov AM, Belyaev FS, Volkov AE, Belyaev SP. Simulation of recoverable strain variation during isothermal holding of the Ni51Ti49 alloy under various regimes. *Letters on Materials*. 2023;13(1): 33–38.
31. Volkov AE, Belyaev FS, Volkova NA, Vukolov EA, Evard ME, Rebrov TV. The effect of martensite stabilization in titanium nickelide after various methods of pre-deformation: simulation with a single set of constants. *Materials Physics and Mechanics*. 2024;52(4): 91–99.
32. Belyaev FS, Volkov AE, Vukolov EA, Evard ME, Kudrina KV, Starodubova MS. Influence of latent heat and heat exchange conditions on tension behavior of shape memory alloy specimen. *Materials Physics and Mechanics*. 2024;52(5): 18–28.
33. Belyaev FS, Volkov AE, Evard ME, Volkova NA. A Microstructural model of SMA with Microplastic Deformation and Defects Accumulation: Application to Thermocyclic Loading. *Materials Today: Proceedings*. 2015;2(3): S583–S587.
34. Volkov AE, Belyaev FS, Evard ME, Volkova NA. Model of the Evolution of Deformation Defects and Irreversible Strain at Thermal Cycling of Stressed TiNi Alloy Specimen. *MATEC Web of Conferences*. 2015;33: 03013.

About Authors

Fedor S. Belyaev
Candidate of Physical and Mathematical Sciences
Senior Researcher (Saint Petersburg State University, St. Petersburg, Russia); Senior Researcher (Institute for Problems in Mechanical Engineering of the Russian Academy of Sciences, St. Petersburg, Russia)

Aleksandr E. Volkov
Doctor of Physical and Mathematical Sciences
Professor (Saint Petersburg State University, St. Petersburg, Russia)

Daniil F. Gorbachenko
Student (St. Petersburg State University, St. Petersburg, Russia)

Margarita E. Evard
Candidate of Physical and Mathematical Sciences
Associate Professor (Saint Petersburg State University, St. Petersburg, Russia)